ACS APPLIED NANO MATERIALS

www.acsanm.org Article

Silica Nanoparticles Coated with Smaller Au Nanoparticles for the Enhancement of Optical Oxygen Sensing

Wenwen Yin, Jiajie Sui, Guozhong Cao, and Dana Dabiri*

Cite This: *ACS Appl. Nano Mater.* 2021, 4, 14146−14152 Read Online

ACCESS | Metrics & More | Article Recommendations | Supporting Information

ABSTRACT: In the vicinity of metal nanostructures, phosphorescent intensity can be greatly enhanced through the localized surface plasmon resonance (LSPR). The enhancement of phosphorescence intensity in noble-metal nanoparticle (NP) systems is highly dependent on the overlap of the absorbance peak of a noble metal with that of phosphorescent dyes. When the peak of the NPs' absorption spectra has a maximum overlap with that of these dyes, the phosphorescence enhancement is the largest. Here, we use a seeded growth method to synthesize SiO_2/Au NPs with tunable plasmonic resonance and compare their phosphorescence enhancement for an oxygen range of 0−21%. The measurement sensitivity of oxygen is strongly dependent on the enhancement of phosphorescence. When used with PtTFPP, when the absorbance peak of the SiO_2/Au NPs has a maximum overlap with that of PtTFPP, the phosphorescence enhancement factor is as high as 7; the sensitivity of oxygen concentration is as high as 75. Moreover, we also optimize the performance by varying the number of NPs to eliminate the nonradiative energy-transfer (NRET) process and self-quenching.

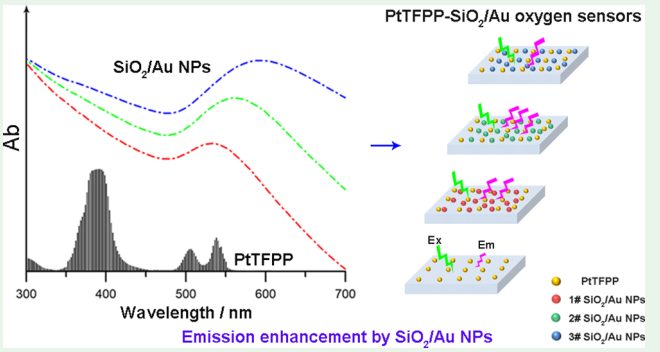

KEYWORDS: *metal-enhanced luminescence, luminescence enhancement, tunable plasmonic resonance peak, sensitivity, oxygen sensors, nanoparticles*

1. INTRODUCTION

Optical oxygen sensors based on the quenching of luminescence emitted from dyes have experienced increasing success in the past decades since their introduction to detecting oxygen.[1,2] These optical oxygen sensors exhibit several advantages such as unmatched sensitivity, remote sensing capabilities via fiber optics, noninvasiveness, and low toxicity,[3−6] which have been successfully used both in scientific and commercial terms.[7−9] However, the response of optical oxygen sensors always faces many problems in actuality when the dye displays weak emission intensity to variations of oxygen concentrations.[10] While, in the vicinity of metal nanostructures, plasmon excitation providing enhanced optical fields can greatly enhance the emission intensity.[11−15] Metal-enhanced luminescence (MEL) can not only provide enhanced emissions but also expand the field of dyes by incorporating weak quantum emitters, which has been proved to be an efficient method to increase luminescence sensitivity and intensity in optical oxygen sensors.[16−18] Chu's group fabricated a metal-enhanced optical oxygen sensor. This sensor comprises an optical fiber that was coated at one end with platinum(II) meso-tetrakis (pentafluorophenyl) porphyrin (PtTFPP) and silver-coated silica nanoparticles (NPs) in an n-octyltriethoxysilane (octyl-triEOS)/tetraethylorthosilane (TEOS) composite xerogel.[16] With metal NPs, the Pt(II)-doped oxygen sensors' sensitivity was eight times higher than that of Pt(II)-doped oxygen sensors. Yin et al. added silica-coated Ag NPs to PtTFPP dyes in pressure-sensitive paints to enhance the luminescence intensity. In an ethanol solution, the luminescence intensity-enhanced factor is 3.[18] Our group prepared a series of SiO_2@Ag with tunable plasmonic resonance and embedded in silica gels containing PtTFPP dyes to measure its variation with respect to oxygen concentration. The SiO_2@Ag-Pt(II)-doped oxygen sensors exhibit high sensitivity, 7.7 times higher than that of Pt(II)-doped oxygen sensors.[19] The higher enhancement and sensitivity of the emission intensity of the metal-based oxygen sensors can be attributed to the augmented emission, resulting from the local field enhancement effects and increased emission rate by surface plasmon coupled emission; this can increase both the fluorescence intensity and the quantum yield. The sensitivity and intensity in metal-based oxygen sensors are affected by many parameters, for example, morphologies and sizes of the dyes

Received: October 19, 2021
Accepted: November 16, 2021
Published: December 6, 2021

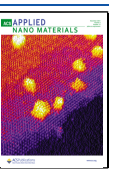

https://doi.org/10.1021/acsanm.1c03391
ACS Appl. Nano Mater. 2021, 4, 14146−14152

Scheme 1. Fabrication of PtTFPP-SiO_2/Au NP-Based Oxygen Sensors

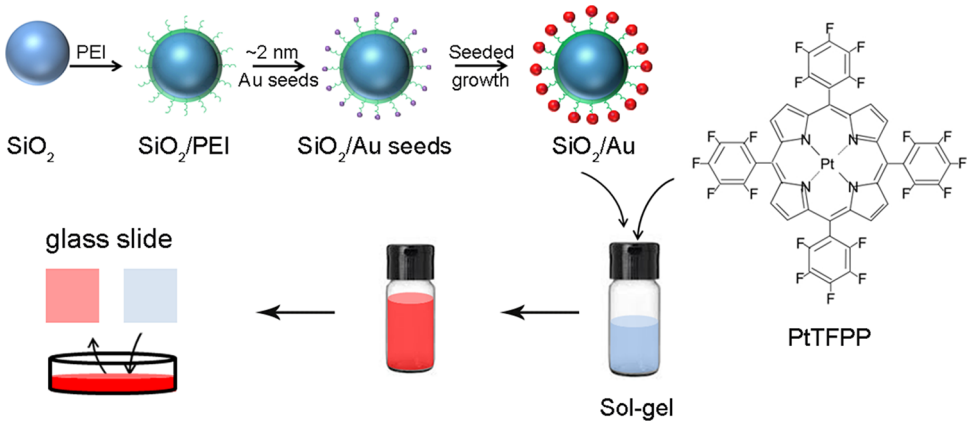

and metal NPs, especially spectra overlap of the metal localized surface plasmon resonance (LSPR) with the excitation spectra. Our results of SiO_2@Ag with tunable plasmon resonance in oxygen sensors have clearly indicated that the emission intensity of MEL-based optical oxygen sensors is strongly correlated with the degree of the spectral overlap between the plasmon resonance of the noble-metal NPs and the absorption peak of luminescence dyes.[19−23] The greatly enhanced intensity will result in more accurate measurements at lower O_2 concentrations, demonstrating that MEL-based oxygen sensors will highly contribute to the field of optical oxygen sensors.

Among various metal materials, silver nanostructures produce the strongest plasmon resonance. It has long been recognized that the use of silver may lead to more sensitive surface plasmonic resonance (SPR)-sensing devices than any other noble-metal materials.[24−27] However, poor chemical and structural stability of silver nanostructures have become the main issue that prevents broad use of silver in SPR sensing.[28−31] In silver-based optical oxygen sensors, the same problem associated with poor stability also exists, which limits the long-term use of silver-based oxygen sensors. Compared with silver, gold displays much weaker LSPR but excellent stability. Thus, Au-based oxygen sensors can be a good alternative compared with Ag-based oxygen sensors. To explore this potential, we first use the same seeded growth method for SiO_2/Ag NPs to synthesize SiO_2/Au NPs.[32] Second, we further make full use of the samples' tunable plasmonic resonance and show its application in an oxygen sensor to amplify the phosphorescence intensity and sensitivity.

2. RESULTS AND DISCUSSION

The seeded growth method is typically used to synthesize SiO_2/Au NPs. This is composed of two steps. The first step is to deposit nucleus seeds on the functionalized SiO_2 surface, and the second step is to grow Au shells over these nucleus seeds.[33] In our work, we focus on investigating how to enhance the emission intensity and sensitivity in MEL-based oxygen sensors. The seeded growth method is just one of the preparation methods for SiO_2/Au NPs. The method is advantageous for preparing nanostructures that have narrow size distributions. In general, the SiO_2 NPs' surface must be functionalized with various organosilanes containing amino (-NH_2) or mercapto (-SH) groups. This will allow for the deposition or adsorption of metal seeds on SiO_2 NPs before following up with growing Au shells.[34] The full surface group modification of SiO_2 NPs is the key to achieving uniform and complete Au shell coating. This is obtained using a slow-growth approach using multiple or slow addition of $HAuClO_4$ to the seed-coated SiO_2 NP suspensions that contain reducing agents.[35,36] In this work, we used polyethyleneimine (PEI) to easily adsorb dense Au seeds on the surface of silica and sequentially add growth solutions containing $HAuClO_4$ for growing Au shells on the SiO_2 NPs, as shown in Scheme 1. This is the most convenient synthesis route for preparing SiO_2/Au NPs with good dispersibility, controllable Au shell, and fast preparation.[37]

The synthesis procedure for obtaining monodisperse SiO_2/Au NPs is as follows: we prepared SiO_2 with 300 nm diameter NPs (Figure 1b) using a modified Stöber method.[38] We treated the SiO_2 NPs ultrasonically with PEI solution, which resulted in PEI-coated SiO_2 NPs. We prepared the SiO_2/Au seeds by adsorbing Au NPs on the PEI layer of SiO_2 NPs using

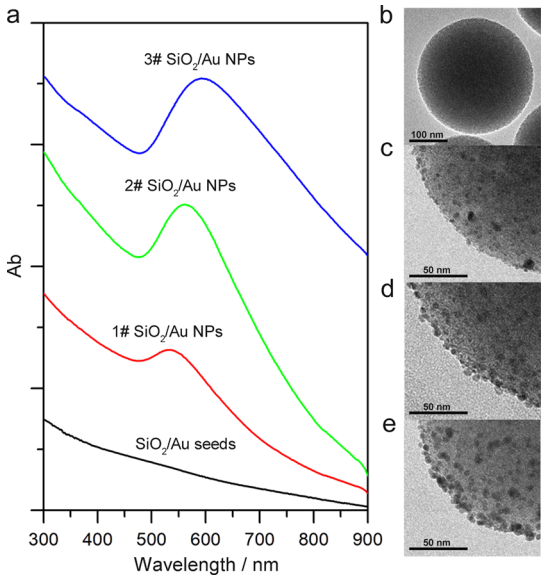

Figure 1. (a) UV−vis spectra of SiO_2/Au prepared by SiO_2-THPC-Au seeds reacted with 0 mL (SiO_2/Au seeds), 20 mL (1# SiO_2/Au), 60 mL (2# SiO_2/Au), and 100 mL (3# SiO_2/Au) of growth solution containing $HAuClO_4$; (b) SiO_2 TEM images; (c) 1# SiO_2/Au TEM images; (d) 2# SiO_2/Au TEM images; and (e) 3# SiO_2/Au NPs TEM images.

https://doi.org/10.1021/acsanm.1c03391
ACS Appl. Nano Mater. 2021, 4, 14146−14152

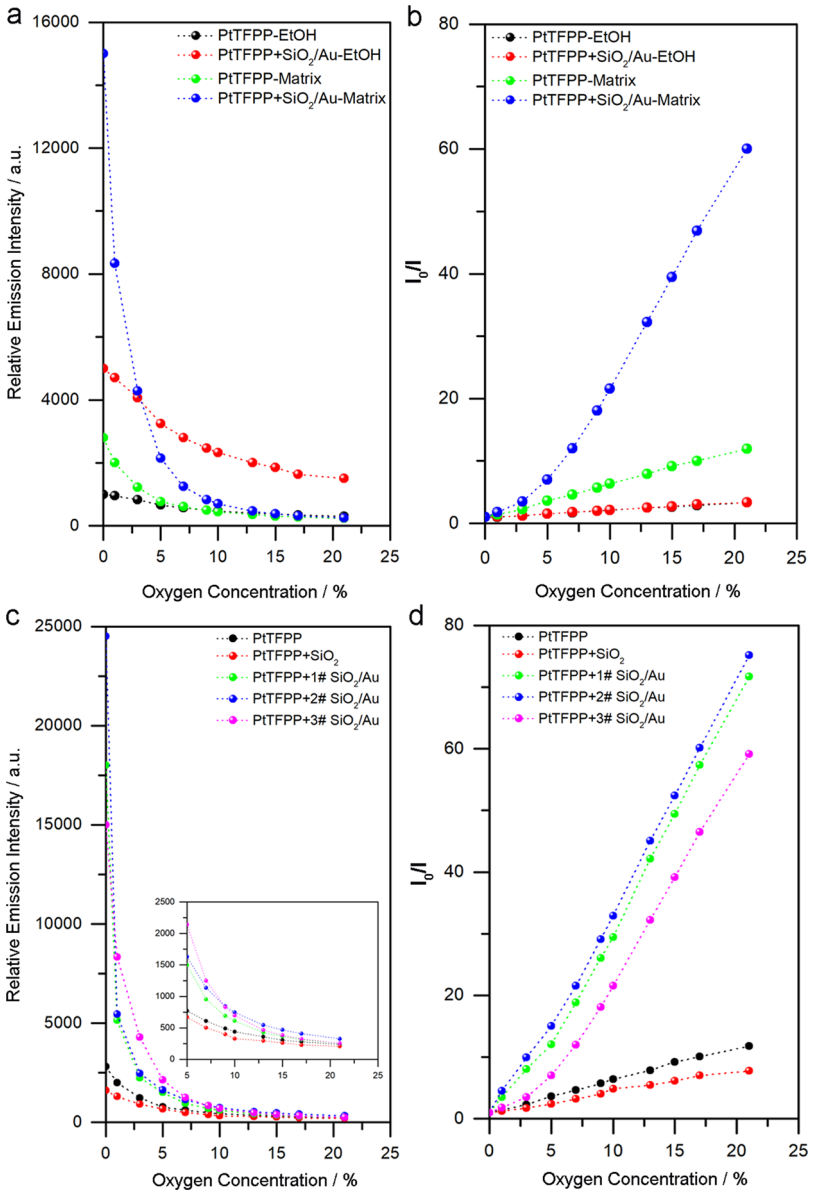

Figure 2. (a) Emission intensity at different oxygen concentrations; (b) Stern–Volmer plots for PtTFPP-based oxygen sensors and PtTFPP and MEP-oxygen sensors mixed with 3# SiO_2/Au NPs in different matrices, in the sol–gel matrix or ethanol, at different oxygen concentrations (0–21%); (c) emission intensity at different oxygen concentrations; (d) Stern–Volmer plots of the Pt-based oxygen sensor and SiO_2/Au-Pt-based oxygen sensors at different oxygen concentrations.

electrostatic attraction between the Au NPs and the $-NH_2$ groups of PEI, as stated in the literature.[37] Finally, by reducing the plating solution using formaldehyde (0.05 mL, 37%) under the stabilization of sodium citrate (0.2 mL, 0.1 M), the SiO_2/Au NPs were rapidly developed. The plating solution was first prepared by adding 7.5 mL of 25 mM $HAuCl_4$ in 500 mL of 1.8 mM K_2CO_3 aqueous solution and stored for a minimum of 24 h before use.[37] We formed the uniform Au shells on the exterior of the SiO_2 NPs using the isotropic growth of all Au seeds under sonication. This was achieved in 5 min. In order to obtain SiO_2/Au NPs with a controllable plasmonic peak in a wide range, we vary the plating solution from 20 mL (1# SiO_2/Au) and 60 mL (2# SiO_2/Au) to 100 mL (3# SiO_2/Au). Figure 1 shows the ultraviolet–visible (UV–vis) spectra of these products with different volumes of growth solution dispersed in deionized (DI) water. As shown in Figure 1a, there is no peak of SiO_2/Au seeds without $HAuClO_4$ growth solution. After the injection of 20 mL of growth solution and the reduction reagent of 0.05 mL of formaldehyde (37%) into 1 mL of SiO_2/Au seed (0.1 mg/mL) suspension, the reduction of Au^{3+} was initiated. The absorbance peak located at 530 nm (1# SiO_2/Au NPs) appears, which indicates the formation of Au NPs on the SiO_2 surface.[37] As the volume of the growth solution increases to 60 (2# SiO_2/Au) and 100 mL (3# SiO_2/Au), the absorbance peaks red-shifted to 600 nm, and the intensity increased significantly. The main reason for the different plasmonic peaks of SiO_2/Au samples prepared with different amounts of growth solution was that as the growth solution increases, the size of Au NPs increases; the interparticle distance was shortened, thereby enhancing plasmonic coupling. Both the increased size of Au NPs and plasmonic coupling lead to the redshift and broad absorption of incident visible light. In this work, the SiO_2 nanospheres we prepared were 300 nm (Figure 1b). As the SiO_2/Au

https://doi.org/10.1021/acsanm.1c03391
ACS Appl. Nano Mater. 2021, 4, 14146–14152

nanospheres prepared with the growth solution increases from 20 to 100 mL (Figure 1c−e), the size of Au NPs on the SiO_2 surface is estimated to be 8 nm (1# SiO_2/Au), 10 nm (2# SiO_2/Au), and 12 nm (3# SiO_2/Au), separately. The amount of Au NPs on SiO_2 nanospheres also increases. Thus, the nanogap between Au NPs on the surface of SiO_2 nanospheres decreased. Using this method, the Au NPs coating on the SiO_2 NPs can be varied from the sparse coating of small Au NPs (Figure 1c) to densely coated and uniform Au NPs (Figure 1e).

The fabrication of oxygen sensors is as shown in the scheme: the prepared SiO_2/Au NPs were uniformly mixed with PtTFPP dyes and composite sol−gel solution; then, the glass slides were immersed in the mixture and dried. There are many good polymer matrices used in oxygen sensors, including polydimethylsiloxane,[39] ethyl cellulose,[40] and hydroxymethyl cellulose.[6,41−43] We just selected the sol−gel in Chu's report to fabricate PtTFPP-based oxygen sensors and investigate the emission enhancement of SiO_2/Au NPs. Oxygen sensors without matrices were prepared with ethanol instead of the sol−gel solution. As shown in Figure 2a, the Pt-based oxygen sensors' emission intensity with EtOH is around three times lower than that of the sensors with the sol−gel matrix at 0% O_2, which indicates that the sol−gel matrix is beneficial for the measurement of oxygen at lower concentrations in the system. With the addition of SiO_2/Au NPs (3# SiO_2/Au) in the oxygen sensors, the intensity of the Pt-NPs based oxygen sensors in EtOH is around 5 times higher than that of the Pt-based oxygen sensors in EtOH throughout the 0−21% O_2 range. In the sol−gel matrix, the luminescence intensity of Pt-NP-based oxygen sensors is five times higher than that of Pt-based oxygen sensors at 0% O_2 and almost the same at 21% O_2. These data show that the emission intensity of oxygen sensors can be greatly enhanced by the SiO_2/Au NPs. The different intensity enhancement of NPs in the matrix and EtOH at different concentrations of O_2 might be caused by the diffusion rate of oxygen in the sol−gel solution and EtOH. The enhancement factor (I_o/I_{O2}: the ratio of intensity at 0% via different oxygen concentrations) of the Pt-based oxygen sensors, with and without NPs, in ethanol solution is almost the same (Figure 2b); the intensity of Pt-based oxygen sensors with NPs within the matrix is five times higher than that without NPs. These data further indicate that the sol−gel is beneficial for the performance of Pt-based oxygen sensors.

The performance of Pt-based oxygen sensors mixed with 1#, 2#, and 3# SiO_2/Au samples were tested and compared. The performance of Pt-based oxygen sensors without NPs was also tested as a comparison. Figure 2c shows that the oxygen sensors' relative phosphorescence intensities decrease as the oxygen concentration increases. In addition, the phosphorescence intensities of Pt-SiO_2/Au-based oxygen sensors are higher than those of Pt-based oxygen sensors at the same concentrations of oxygen because of the metal-enhanced phosphorescence of SiO_2/Au. Among these SiO_2/Au samples, the phosphorescence intensity of the 2# SiO_2/Au-Pt-based oxygen sensor, which is prepared with 60 mL of $HAuClO_4$ growth solution at 0.0% O_2, is the highest than the other SiO_2/Au samples, while the intensity of the oxygen sensors with these SiO_2/Au samples is closer in value at 21% O_2. In order to obtain a clear insight into the difference in the oxygen sensors, we increase the emission intensity at 5−21%. As shown in the inset of Figure 2a, at 5−10%, the emission intensity decreases in the order 3# > 2# > 1#; at 10−21%, and the emission intensity of 2# is higher than those of 3# and 1#. The emission of the oxygen sensors with SiO_2/Au is observed to be still brighter than that of the oxygen sensors at a higher concentration of oxygen. As a comparison, we also fabricate oxygen sensors just mixed with SiO_2. The PtTFPP-SiO_2 oxygen sensors' intensity is much weaker than that of the PtTFPP-oxygen sensors; this further shows that the oxygen sensors' enhancement is attributed to the metal-enhanced phosphorescence of Au.

The slope of the Stern−Volmer plot, K_{sv}, based on the ratio of $I_o/I_{[O2]}$ divided by the oxygen concentration provides a measure for the relative sensitivity of the oxygen sensors. At 0−5% O_2, the plots of Pt-NP-based oxygen sensors are nonlinear. From 7−21% O_2 concentrations, the slopes are constant, ranging from 3.36 for 3# and 3.77 for 1# to 3.83 for 2#. Compared with the slope of the Pt-based oxygen sensor, 0.51, this shows a 6.6−7.5-fold increase in sensitivity. The maximum (I_0/I) for the enhanced curves range from 59−75, which when compared with the maximum (I_0/I) of the Pt-based oxygen sensor, 11, shows a 5.3−6.8-fold increase in the maximum attainable I_0/I. The different sensitivities of these samples can be predominantly attributed to the different phosphorescence intensity profiles of the PtTFPP-SiO_2/Au-based oxygen sensors, that is, to say, higher intensities at 0% O_2 (I_o) and almost the same intensities at 21% O_2 will lead to larger slopes and therefore higher sensitivities. The different enhancement of phosphorescence intensities is caused by the different absorbance peaks of different SiO_2/Au NPs, resulting in different overlap between the excitation spectra of the dyes and the LSPR of the SiO_2/Au NPs. The dominant excitation of PtTFPP is at 392 nm, and compared with the UV−vis spectra of these SiO_2/Au samples, the 2# sample has the maximum overlap and thus the highest enhancement factor. These data further support experimental evidence that the intensity of dyes enhanced by the SiO_2/Au NPs relies strongly on the overlap between the excitation spectra properties of the dye with the LSPR of the NP, which is consistent with our previous findings using the seeded growth of SiO_2@Ag with tunable plasmon resonances.[18] Compared with that of the PtTFPP-SiO_2/Ag-based oxygen sensors, the sensitivity of PtTFPP-SiO_2/Au-based oxygen sensors is slightly lower *at low concentrations (0−5%) but almost the same at 5−21%* (Figure S2). The difference can be explained as follows: the absorption spectrum of the PtTFPP has a Soret band (S_0 to S_2 transition) at 392 nm and two Q bands (S_0 to S_1 transition) at 508 and 541 nm, respectively. The absorbance peak of SiO_2@Ag is mainly localized at 450 nm, while the absorbance peak of SiO_2/Au is mainly localized at 550 nm. It can be seen that the absorbance peak of SiO_2@Ag is more overlapped with that of PtTFPP dyes. Furthermore, the silver NPs display stronger LSPR with higher plasmon energy and more intense local electric field enhancement than gold NPs. In addition, the SiO_2@Ag NPs are more easily oxidized at higher concentrations of oxygen, and the diffusion of oxygen in the sol−gel system will lead to the surface oxidation of SiO_2@Ag, finally resulting in the weakened emission intensity at higher concentrations of oxygen. While at higher concentrations of oxygen, the SiO_2/Au NPs are stable, the SiO_2/Au NP-based oxygen sensors can emit brighter luminescence. Based on these results, both the LSPR of the NPs matched well with the excitation spectra of the dyes, and the stability of NPs is crucial to the intensity enhancement in oxygen sensors. That is to say, in addition to the PtTFPP dye, the intensity of other dyes

https://doi.org/10.1021/acsanm.1c03391
ACS Appl. Nano Mater. 2021, 4, 14146−14152

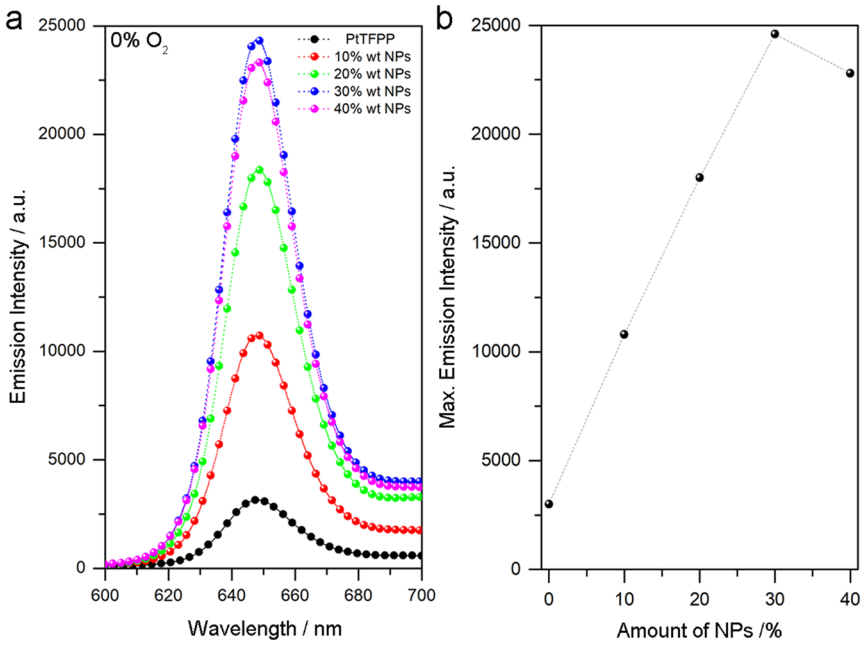

Figure 3. (a) Phosphorescence intensity; (b) maximum phosphorescence intensity of PtTFPP at different volumes of 2# SiO_2/Au measured at 0% oxygen concentration.

including fluorescent dyes can also be enhanced with matched NPs. The role of SiO_2 NPs is to prepare NPs with a wide absorbance peak in visible light.

To optimize the performance of SiO_2/Au-Pt-based oxygen sensors, we further investigate the dependence of phosphorescence intensity on the number of SiO_2/Au NPs. As shown in Figure 3a, the peak phosphorescence intensity of Pt-based oxygen sensors (fixed volume of 0.2 mg/mL PtTFPP at 0.2 mL) at 0% oxygen concentration is around 3000. As the volume of SiO_2/Au increases from 10 to 30% wt, the peak intensity increases from 11,000 to 24,000; while the number of SiO_2/Au further increases to 40%, the peak intensity decreases to 23,000. Figure 3b shows that this trend can be clearly seen in the maximum phosphorescence intensity plot. These data show that the phosphorescence intensity of SiO_2/Au-Pt-based oxygen sensors is highly dependent on the number of SiO_2/Au NPs. In the fluorescein system, there are resonance energy transfer between fluorescein molecules (homo RET), which is called self-quenching and nonradiative energy transfer (NRET) to the NPs.[39] In our SiO_2/Au-PtTFPP systems, if the PtTFPP molecules are too close to each other, self-quenching will occur. In addition, if the PtTFPP molecules are too close to the SiO_2/Au NPs, there will be NRET to the NPs. Both the self-quenching (RET) and NRET will weaken the emission from the dyes. Only when these distances are optimized, these losses can be eliminated so that the phosphorescence emission under the effect of the electromagnetic field of NPs can be significantly enhanced. In this case, when the volume of NPs is less than 30%, the number of NPs is not enough to accomplish this: the dyes are surrounded by more dye and less NPs, leading to more self-quenching and therefore less MEL. At 30% NPs, the dyes are mostly surrounded by NPs, the MEL is strongest, and thus the intensity is the brightest. When the volume of NPs is further increased to 40%, the NRET is dominated by the NPs, resulting in a decrease in phosphorescence intensity. Therefore, 30 wt % NPs by volume is the optimal amount for the SiO_2/Au-PtTFPP-based oxygen sensors.

The photostability of Pt-based oxygen sensors was tested by irradiation of the oxygen sensors with 405 nm laser at room temperature for 5 h, as shown in Figure 4. After illumination

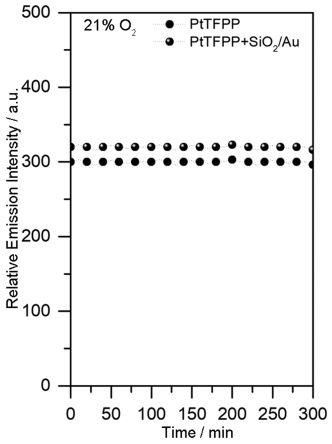

Figure 4. Photostability of PtTFPP-based oxygen sensors.

for 5 h, the relative phosphorescence intensity of the Pt-based oxygen sensor and the 1# SiO_2/Au-Pt-based oxygen sensor at 21% O_2 remains stable at 300 and 320, respectively, with no signs of decay. This is because the fluorophenyl groups of the PtTFPP (PtTFPP has four fluorophenyl groups that are connected to its porphyrin) are impervious to oxidation/reduction, thereby making the PtTFPP molecules stable against photo-oxidation/reduction. In addition, the SiO_2/Au is also very stable; this, therefore, increases the photostability of Pt-based oxygen sensors.

3. CONCLUSIONS

In this work, we fabricated PtTFPP-based oxygen sensors with SiO_2/Au NPs. Under the MEL effect of NPs, both the

https://doi.org/10.1021/acsanm.1c03391
ACS Appl. Nano Mater. 2021, 4, 14146−14152

sensitivity and intensity of oxygen sensors can be greatly enhanced in a wide range of oxygen concentrations. The intensity of dyes enhanced by the NPs relies strongly on the overlap between the LSPR of the NPs with the excitation spectra properties of the dye. If one were to use other dyes that are often used in luminescent oxygen sensing (e.g., PtOEP), it would be important to design and fabricate NPs to maximize the overlap between the NPs' LSPR and the dye's excitation spectra. There are some inherent limitations from solution processing, such as the need to control the space/distance between Au NPs and to prevent them from aggregation. Because of such current material processing challenges, we believe the sensitivities achieved in this work are far from the maximum value. This new type of noble-metal-based oxygen sensors and the approach for use with other luminescent oxygen sensors offer us accurate measurements ranging from a low oxygen concentration (0%) to atmospheric oxygen concentrations (21%), which is a great milestone in the development of ultrasensitive oxygen sensors.

4. EXPERIMENTAL SECTION

4.1. Synthesis of SiO_2 Nanospheres. The synthesis of SiO_2 nanospheres was performed, as described in our previous publication.[18]

4.2. Synthesis of SiO_2/Au. The synthesis of SiO_2/Ag described in our previous publication[18] was adjusted for the use of Au. Here, we dispersed 0.6 g of SiO_2 in 60 mL of PEI (1 wt %) solution, and then, the solution was stirred for 4 h. The SiO_2 nanospheres from the previous step were washed three times with water and then placed in 6 mL of water (0.1 g/mL). The sample (1 mL) was then pipetted to 10 mL of tetrakis-(hydroxymethyl) phosphonium chloride (THPC)-Au seed solution and sonified for 1 h and then stirred overnight. The solution was then centrifuged and dispersed in water. Baiker's method was used to synthesize the THPC-Au seeds: 41 mL of water, 1.35 mL of NaOH (0.2 M), and 0.90 mL of THPC aqueous solution (1.2 mM) were mixed and stirred for 10 min, after which 1.80 mL of the aqueous solution of chloroauric acid (25 mM) was quickly added. Then, the resulting solution was aged for a minimum of 2 weeks at 4 °C before it was used.

The seed-mediated growth was then carried out to deposit Au onto the Au seeds attached to the SiO_2 particles. A plating solution was first prepared by adding 7.5 mL of 25 mM HAuCl4 in 500 mL of 1.8 mM K_2CO_3 aqueous solution and stored for at least 24 h before use. The above SiO_2/Au seed solution was added to 20 mL of the plating solution, stirred for 5 min, and mixed with 0.2 mL of 100 mM trimethyl sodium citrate and 0.05 mL of formaldehyde (37%), and then stirred for 10 min. Finally, we centrifuged the sample and then washed it with water three times. For the growth procedure, after centrifuging and washing, the prepared SiO_2/Au samples were added to 20 mL of plating solution and mixed with TSC and formaldehyde multiple times to prepare 1# (1 time), 2# (3 times), and 3# (5 times).

4.3. Fabrication of SiO_2/Au-Based Oxygen Sensors. Octyl-triEOS/TEOS composite sol−gel was used as the matrix material in the pressure-sensitive paint. The sol−gel was prepared by mixing 0.20 mL of octyl-triEOS and 4.0 mL of TEOS; this forms the precursor solution using Chu's method. We then added 1.25 mL of EtOH and 0.40 mL of HCl (0.1 M) to this solution, which catalyzed the ORMOSIL reaction. We then magnetically stirred the solution for 1 h at room temperature. We then added 0.10 mL of Triton-X-100 so that the silica sol's homogeneity would be improved. Next, we added 20 mg of SiO_2/Au to 0.50 mL of PtTFPP/EtOH (0.2 mg/mL), and the solution was stirred for 12 h. Next, we added 0.50 mL of the composite sol−gel solution to the dye solution. Lastly, we capped the solution and magnetically stirred it for another 12 h. Before testing the response of this formulation to varying oxygen concentrations, the glass slide (2 × 2 cm^2) was immersed in the solution for 10 min and left to stabilize under ambient air conditions for 24 h.

ASSOCIATED CONTENT

Supporting Information

The Supporting Information is available free of charge at https://pubs.acs.org/doi/10.1021/acsanm.1c03391.

UV−vis absorption spectra of PtTFPP and 1−3# SiO_2/Au NPs (PDF)

Plot showing the wavelength of PtTFPP against Ab (TIF)

AUTHOR INFORMATION

Corresponding Author

Dana Dabiri − *Department of Aeronautics & Astronautics, University of Washington, Seattle, Washington 98195-2120, United States;* orcid.org/0000-0003-3573-6897; Email: dabiri@uw.edu

Authors

Wenwen Yin − *Department of Aeronautics & Astronautics, University of Washington, Seattle, Washington 98195-2120, United States;* Present Address: Sun Yat-sen University, 2 Daxue Road, Zhuhai 519000, China; orcid.org/0000-0003-2082-8537

Jiajie Sui − *Department of Materials and Engineering, University of Washington, Seattle, Washington 98195-2120, United States;* Present Address: University of Wisconsin-Madison, 1500 Engineering Drive, Madison, WI 53715, United States; orcid.org/0000-0001-6580-1886

Guozhong Cao − *Department of Materials and Engineering, University of Washington, Seattle, Washington 98195-2120, United States;* orcid.org/0000-0001-6539-0490

Complete contact information is available at: https://pubs.acs.org/10.1021/acsanm.1c03391

Notes

The authors declare no competing financial interest.

ACKNOWLEDGMENTS

The U.S. Army Research Office under Grant No. W911NF-18-1-0143 overseen by Dr. Matthew Munson financially supported this effort, for which we are grateful. We also acknowledge the support of the UW CoMotion Commercialization Fellowship Program for W.Y.

REFERENCES

(1) Kochmann, S.; Baleizão, C.; Berberan-Santos, M. N.; Wolfbeis, O. S. Sensing and Imaging of Oxygen with Parts per Billion Limits of Detection and Based on the Quenching of the Delayed Fluorescence of 13C70 Fullerene in Polymer Hosts. *Anal. Chem.* **2013**, *85*, 1300−1304.

(2) Lehner, P.; Staudinger, C.; Borisov, S.; Klimant, I. Ultra-sensitive optical oxygen sensors for characterization of nearly anoxic systems. *Nat. Commun.* **2014**, *5*, 4460.

(3) Alexandrovskaya, Y. A.; Melnikov, P. V.; Safonov, A. V.; Naumova, A. O.; Zaytsev, N. K. A comprehensive study of the resistance to biofouling of different polymers for optical oxygen sensors. The advantage of the novel fluorinated composite based on core-dye-shell structure. *Mater. Today Commun.* **2020**, *23*, No. 100916.

(4) Lei, B.; Li, B.; Zhang, H.; Lu, S.; Zheng, Z.; Li, W.; Wang, Y. Mesostructured Silica Chemically Doped with RuII as a Superior Optical Oxygen Sensor. *Adv. Funct. Mater.* **2006**, *16*, 1883−1891.

(5) Lim, C. J.; Lee, S.; Kim, J. H.; Kil, H. J.; Kim, Y. C.; Park, J. W. Wearable, Luminescent Oxygen Sensor for Transcutaneous Oxygen Monitoring. *ACS Appl. Mater. Interfaces* **2018**, *10*, 41026−41034.

(6) Wang, X. D.; Wolfbeis, O. S. Optical methods for sensing and imaging oxygen: materials, spectroscopies and applications. *Chem. Soc. Rev.* **2014**, *43*, 3666−3761.
(7) Wolfbeis, O. S. Luminescent sensing and imaging of oxygen: Fierce competition to the Clark electrode. *BioEssays* **2015**, *37*, 921−928.
(8) Ferreira, F.; Luxardi, G.; Reid, B.; Ma, L.; Raghunathan, V.; Zhao, M. Real-time physiological measurements of oxygen using a non-invasive self-referencing optical fiber microsensor. *Nat. Protoc.* **2020**, *15*, 207−235.
(9) Chang, X.; Li, S.; Chu, D. Sensing of Oxygen Partial Pressure in Air with ZnO Nanoparticles. *Sensors* **2020**, *20*, 562.
(10) Liu, P. P.; Guo, M.; Lan, C.; Huang, B.; Yang, S.; Qiu, Y.; Ma, Y. Fluorescence enhancement of strip patterned silver nanoparticle platforms prepared by room-temperature imprinting technique. *Mater. Express.* **2018**, *8*, 272−278.
(11) Liu, R.; Xiao, T.; Cui, W.; Shinar, J.; Shinar, R. Multiple approaches for enhancing all-organic electronics photoluminescent sensors: simultaneous oxygen and pH monitoring. *Anal. Chim. Acta* **2013**, *778*, 70−78.
(12) Gartia, M. R.; Hsiao, A.; Sivaguru, M.; Chen, Y.; Logan Liu, G. Enhanced 3D fluorescence live cell imaging on nanoplasmonic substrate. *Nanotechnology* **2011**, *22*, No. 365203.
(13) Kang, M.; Kim, J. J.; Oh, Y. J.; Park, S. G.; Jeong, K. H. A Deformable Nanoplasmonic Membrane Reveals Universal Correlations Between Plasmon Resonance and Surface Enhanced Raman Scattering. *Adv. Mater.* **2014**, *26*, 4510−4514.
(14) Ayala-Orozco, C.; Liu, J. G.; Knight, M. W.; Wang, Y.; Day, J. K.; Nordlander, P.; Halas, N. J. Fluorescence Enhancement of Molecules Inside a Gold Nanomatryoshka. *Nano Lett.* **2014**, *14*, 2926−2933.
(15) Zhang, J.; Fu, Y.; Liang, D.; Nowaczyk, K.; Zhao, R. Y.; Lakowicz, J. R. Metal-Enhanced Single-Molecule Fluorescence on Silver Particle Monomer and Dimer: Coupling Effect between Metal Particles. *Nano Lett.* **2008**, *8*, 1179−1186.
(16) Chu, C. S.; Sung, T. W.; Lo, Y. L. Enhanced optical oxygen sensing property based on Pt(II) complex and metal-coated silica nanoparticles embedded in sol−gel matrix. *Sens. Actuators B: Chem.* **2013**, *185*, 287−292.
(17) Peak, S. M.; Watkins, A. N. Addition of silica-coated Ag Nanoparticles to enhance luminescence intensity of pressure-sensitive paints. *ACS Appl. Nano Mater.* **2020**, *3*, 9813−9821.
(18) Yin, W. W.; Chen, J. X.; Sui, J. J.; Dabiri, D.; Cao, G. Z. *Luminescence and Sensitivity Enhancement of Oxygen Sensors through tuning the Spectral Overlap Between Luminescent dyes and SiO2@Ag Nanoparticles*. Nano Select 2021, DOI: 10.1002/nano.202100131.
(19) Yuan, H.; Khatua, S.; Zijlstra, P.; Yorulmaz, M.; Orrit, M. Thousand-fold enhancement of single-molecule fluorescence near a single gold nanorod. *Angew. Chem., Int. Ed.* **2013**, *52*, 1217−1221.
(20) Su, L.; Yuan, H. F.; Lu, G.; Rocha, S.; Orrit, M.; Hofkens, J.; Uji-i, H. Super-resolution localization and defocused fluorescence microscopy on resonantly coupled single-molecule, single-nanorod hybrids. *ACS Nano* **2016**, *10*, 2455−2466.
(21) Chen, Y.; Munechika, K.; Ginger, D. Dependence of fluorescence intensity on the spectral overlap between fluorophores and plasmon resonant single silver nanoparticles. *Nano Lett.* **2007**, *7*, 690−696.
(22) Theodorou, I. G.; Jiang, Q.; Malms, L.; Xie, X.; Coombes, R. C.; Aboagye, E. O.; Porter, A. E.; Ryan, M. P.; Xie, F. Fluorescence enhancement from single gold nanostars: towards ultra-bright emission in the first and second near-infrared biological windows. *Nanoscale* **2018**, *10*, 15854−15864.
(23) Camposeo, A.; Persano, L.; Manco, R.; Wang, Y.; del Carro, P.; Zhang, C.; Li, Z.; Pisignano, D.; Xia, Y. Metal-enhanced near-infrared fluorescence by micropatterned gold nanocages. *ACS Nano* **2015**, *9*, 10047−10054.
(24) Giner-Casares, J. J.; Liz-Marzán, L. M. Plasmonic nanoparticles in 2D for biological applications: Toward active multipurpose platforms. *Nano Today* **2014**, *9*, 365−377.
(25) Tang, F.; He, F.; Cheng, H.; Li, L. Self-assembly of conjugated polymer-Ag@SiO2 hybrid fluorescent nanoparticles for application to cellular imaging. *Langmuir* **2010**, *26*, 11774−11778.
(26) Gao, C.; Lu, Z.; Liu, Y.; Zhang, Q.; Chi, M.; Cheng, Q.; Yin, Y. Highly stable silver nanoplate for surface plasmon resonance biosensing. *Angew. Chem., Int. Ed.* **2012**, *51*, 5629−5633.
(27) Gao, C.; Hu, Y.; Wang, M.; Chi, M.; Yin, Y. Fully alloyed Ag/Au nanospheres: combining the plasmonic property of Ag with the stability of Au. *J. Am. Chem. Soc.* **2014**, *136*, 7474−7479.
(28) Cortie, M. B.; McDonagh, A. M. Synthesis and optical properties of hybrid and alloy plasmonic nanoparticles. *Chem. Rev.* **2011**, *111*, 3713−3735.
(29) Kim, M.; Ko, S. M.; Nam, J. M. Dealloying-based facile synthesis and highly catalytic properties of Au core/porous shell nanoparticles. *Nanoscale* **2016**, *8*, 11707−11717.
(30) Zharov, V. P. Ultrasharp nonlinear photothermal and photoacoustic resonances and holes beyond the spectral limit. *Nat. Photonics* **2011**, *5*, 110−116.
(31) Dobrowolska, P.; Krajewska, A.; Gajda-Rączka, M.; Bartosewicz, B.; Nyga, P.; Jankiewicz, B. Application of Turkevich Method for Gold Nanoparticles Synthesis to Fabrication of SiO2@Au and TiO2@Au Core-Shell Nanostructures. *Materials* **2015**, *8*, 2849−2862.
(32) The X@Y is used to signify a core material, X, is covered with a Y shell material. In our work, since the Au nano particles do not form a shell, we introduce a new nomenclature, X/Y, to distinguish between these differences.
(33) Lu, Y.; Zhong, J.; Yao, G.; Huang, Q. A label-free SERS approach to quantitative and selective detection of mercury (II) based on DNA aptamer-modified SiO2@Au core/shell nanoparticles. *Sens. Actuators B: Chem.* **2018**, *258*, 365−372.
(34) Wang, R.; Ji, X.; Huang, Z.; Xue, Y.; Wang, D.; Yang, W. Citrate-Regulated Surface Morphology of SiO2@Au Particles To Control the Surface Plasmonic Properties. *J. Phys. Chem. C* **2016**, *120*, 377−385.
(35) Gomez, L.; Arruebo, M.; Sebastian, V.; Gutierrez, L.; Santamaria, J. Facile synthesis of SiO2−Au nanoshells in a three-stage microfluidic system. *J. Mater. Chem.* **2012**, *22*, 21420−21425.
(36) Wang, K.; Wang, Y.; Wang, C.; Jia, X.; Li, J.; Xiao, R.; Wang, S. Facile synthesis of high-performance SiO2@Au core−shell nanoparticles with high SERS activity. *RSC Adv.* **2018**, *8*, 30825−30831.
(37) Stöber, W.; Fink, A.; Bohn, E. Controlled growth of monodisperse silica spheres in the micron size range. *J. Colloid Interface Sci.* **1968**, *26*, 62−69.
(38) Lakowicz, J. R.; Malicka, J.; D'Auria, S.; Gryczynski, I. Release of the self-quenching of fluorescence near silver metallic surfaces. *Anal. Biochem.* **2003**, *320*, 13−20.
(39) Mao, Y.; Gao, Y.; Wu, S.; Wu, S.; Shi, J.; Zhou, B.; Tian, Y. Highly enhanced sensitivity of optical oxygen sensors using microstructured PtTFPP/PDMS-pillar arrays sensing layer. *Sens. Actuators B: Chem.* **2017**, *251*, 495−502.
(40) Eaton, K. A novel colorimetric oxygen sensor: dye redox chemistry in a thin polymer film. *Sens. Actuators B: Chem.* **2002**, *85*, 42−51.
(41) Mills, A.; Lawrie, K.; Bardin, J.; Apedaile, A.; Skinner, G. A.; O'Rourke, C. An O2 smart plastic film for packaging. *Analyst* **2012**, *137*, 106−112.
(42) Akram, M.; Akhtar, M. H.; Irfan, M.; Tian, Y. Polymer matrix: A good substrate material for oxygen probes used in pressure sensitive paints. *Adv. Colloid Interface Sci.* **2020**, *283*, 102240.
(43) Wolfbeis, O. S. Sensor Paints. *Adv. Mater.* **2008**, *20*, 3759−3763.